Iranian Journal of Astronomy and Astrophysics
Vol. 10, No. 1, Winter 2023, 61–75
©Available online at http://ijaa.du.ac.ir
DOI: 10.22128/ijaa.2023.713.1156
Online ISSN: 2383–403X

Iranian Journal of Astronomy and Astrophysics

Research Paper

Downward and Upward Propagating Magneto-Acoustic Waves Over a Solar Limb Prominence

Neda Dadashi*[1] · Maryam Ghiasi[2]

[1] Department of physics, University of Zanjan, Zanjan, P.O.Box 45371-38791, Iran;
*email: dadashi@znu.ac.ir

[2] Faculty of physics, University of Tabriz, Tabriz, Iran;
email: ghiassimaryam@yahoo.com

Received: 21 August 2023; **Accepted:** 17 September 2023; **Published:** 1 October 2023

Abstract. Prominences are cold and dense chromospheric material suspended in the solar atmosphere with the support of coronal magnetic fields. Oscillatory behavior of a limb core prominence is studied in the AIA 171, 193, 211, 335, and 94 Å passbands of AIA aboard SDO. Vertical oscillations with periods of 34.8, and 40.0 minutes with velocity amplitudes of 4.6, and 5.2 km/s are obtained over the prominence core structure in the all studied channels. These long period oscillation started 54 minutes before an external flare eruption starts to develop over the north side of the studied core prominence, and continued for about two hours. Wave fronts from the Flare Eruption (FE) might be the exciter of these long period oscillation over the entire core prominence. Propagating upward and Downward slow magneto-acoustic waves with velocities in the range of 11.3 to 24.2 km/s are observed over the upper and lower boundaries of the prominence. The multiple rapidly heating and cooling effects, with the time scales less than one minutes, are observed over the propagating peak intensities, which might be the response of the plasma before reaching to a thermal balance between the injected heating flux (through the wave fronts of the FE) and heating loss flux through conduction, radiation, and viscosity.

Keywords: The Sun: corona, The Sun: oscillations, The Sun: filaments, Prominences

1 Introduction

Solar prominences are relatively cold and dense plasma features appear as suspended clouds in the solar atmosphere. There are strong evidences indicating that the balance of the prominence structures against the gravity has magnetic origins [1,2]. Evantually, eruption of these structures could cause the solar flares or Coronal Mass Ejections (CMEs) to happen. Two types of prominences are distinguished as Quiescent prominences, and Active-region prominences. The first one, the most common one, is occurring quite away from the active regions, extending more in height, morphologically wider, having weaker magnetic fields (5-10 G), and longer life-times (even up to 2-3 solar rotation) with a gently erupting end-point. Their temperature and density respect to their surrounding environment are about hundred times smaller and larger. This means that their pressure and temperatures are isolated from

* *Corresponding author*

their surrounding. They usually appear around a Polarity Inversion Line. The magnetic field is mainly horizontal and increases with prominence height. Close to the eruption phase, the magnetic field is getting twisted and the axial component of the magnetic field being prevalent. It is observed that the reconnection could increase the magnetic field twist [3,4]. On the other side, the Active-region prominences, in general, are smaller than quiescent ones with larger magnetic fields (up to 70 G). They show 10 times greater gas pressure, and their life-times usually ranges between a few hours to couple of months [5]. Matter condensing and falling (or coronal rains) are usually observed within them [1,3,5–7].

Pre-eruption oscillations are observed over the prominence filaments in Hα line. Along with these oscillations, the presence of siphon flows and surges are observed, as well [7–10]. They interpreted these events as signatures of magnetic reconnection between the new emerging flux and existing coronal magnetic fields.

Different types of waves, such as standing, quasi-periodic, and propagating have been observed over a wide range of solar atmospheric features (i.e., coronal loops, chromospheric spicules and fibrils, network bright points, prominence filaments, and photospheric sunspot pores, etc.), so far. Oliver 1999 classified the prominence oscillations into small ($< 3\,$km/s) and large ($> 20\,$km/s) velocity amplitude oscillations [11]. Observational signatures of a third intermediate group of oscillations, with velocity amplitudes in the range of 3 to 20 km/s, have been observed more recently. Today, it is evident that the small amplitude oscillations (up to 10 km/s), usually, occur in some part(s) of the prominence and do not relate to flare activities, while, large amplitude oscillations (larger than 10 to 20 km/s) occur over a larger (or the whole) part(s) of the prominence structure and related to high energetic events, like flares and CMEs [2].

Another type of classification is provided by Engvold on 2001b based on the period of the oscillations [6,12]; short periods (3 to 5 minutes), longer periods (12 to 20 minutes), and very long periods (40 to 90 minutes). The first type is related to photospheric p-mode oscillations, while the second and third types are related to fast and slow magneto-acoustic waves, respectively.

Three types of MHD waves are known to propagate in ma cylindrical magnetized plasma; The Fast magneto-acoustic waves, which are transverse in nature, and basically could propagate in any direction. Slow magneto-acoustic modes, that are longitudinal and, therefore, can only transmit the energy in the direction of the magnetic field. Alfvén waves, which are transverse and incompressible, propagate in the magnetic field direction. Therefore, they can not produce any change in the pressure, density, and intensity [3].

Standing waves are the oscillations with fixed nodes, while, the propagating waves are the oscillations with moving nodes. If the wave excitation agent acts only at one side of the oscillatory medium, in a very shorter time with respect to the time needed for the signal to reflects back from the other end of the medium, a propagating wave (or a series of disturbance) could get produced. Propagating waves are important in coronal heating, since they can transfer energy in the solar atmosphere. Upward propagating waves have been observed in the variety of different solar atmospheric features such as, coronal EIT waves, Morton waves, polar plums, polar coronal holes, sunspot penumbra, legs of the fan-like loops in the AR [6,13–21]. Continuous shuffling of photospheric granular or chromospheric supergranular flows could be a source of generating slow upward propagating waves [21,22]. However, very rare cases of downward propagating waves are observed.

The paper is structured as follows: Section 2 presents the observational data properties. In the section 3, the results of the observed prominence oscillations are demonstrated in four separate subsections. Finally, the discussions and summary of the paper are provided in the section 4.

2 Observations and Data Analysis

Level 2 EUV images of the Atmospheric Imaging Assembly (AIA) [23] on board Solar Dynamic Observatory (SDO) are used to study the propagating oscillations over a crescent shape core prominence appeared at the solar West limb on the 2014-04-03 between 13:16:10 to 15:13:09 UT with a step cadence of 12 sec. A Filament Eruption (FE) started to occur on the 14:10:10 UT (54 minutes after starting time of our observation) nearby the structure, on the West limb (centered at $x_{cen}, y_{cen} = 1029'', 144''$) and continued until 17:38:03 UT. Spacial resolution of the AIA images are $0.6''$ per pixel. The 171, 193, 211, 335, 94 Å AIA passband images are used in this study. The standard Solar SoftWare (SSW) is used to analyze the data.

Figure 1 represent the studied prominence in different AIA passbands. White arrows indicate the position of the prominence core above the solar limb. As it was expected form a cool, and dense prominence, the structure looks bright in the cool chromospheric 1700, and 1600 Å channels. However, it looks darker over the other hotter channels (171, 193, 211, 335 Å), since the structure is cold and do not emit in the hotter temperatures.

Figure 2 demonstrates a closer look at the prominence core in AIA 171 Å. To study the emission variation over the dark crescent shape prominence structure, which keeps its crescent shape over the two thirds of our study time, twenty points are selected and marked over the top and below borders of the structure. Linear interpolating the position of the selected points, we made two artificial slits named as S1 (connecting point 1 to 10 on the top border of the structure), and S2 (connecting point 11 to point 20 over the below border of the structure), respectively.

3 Results

Looking to Figure 1, one can estimate the height of the core prominence structure (respect to the solar limb) to be about $50''$ ($\simeq 36$ Mm), which is quite high. The time-distance diagrams over the mentioned slits, S1 and S2, for AIA 171, 193, 211, 335, and 94 Å channels are shown in Figure 3. The white dashed lines demonstrate the starting instance of the Flare Eruption (FE) event that occurred nearby the north side of the studied prominence core.

3.1 Oscillatory pattern over the S1 and S2 slits

Looking to the time-distance plot of the slit S2 in the AIA 171 Å, the lower-left panel, it seems that the dark structure of the prominence moves from upper toward the bottom part of the prominence (form the point 20 toward the point 10) in the first 15 minutes of the study, then it moves back in the opposite direction until about the minute 30 of the study. Tracking the structure in the rest of the study time interval shows an oscillatory pattern along the main axis of the structure. Coherent, and almost similar patterns are also visible in the hotter channels over the slit S2 (bottom panels of Figure 3).

Time-distance plots of the slit S1 (the upper panels of Figure 3) show coherent oscillating patterns in all channels, as well. However, the oscillations looks to be out of phase respect to those of the S1 slit. To have a little more accurate estimation about these apparent oscillations, we tried to sum up the emissions in each time step of the study. As expected, oscillatory light curves obtained. Afterward, we fitted sinusoidal functions to the light curves to obtain the oscillatory periods. The amplitudes of the oscillations are modified afterward, in a by-eye manner. The final fitted curves to track the overall displacements of the dark prominence structure are over-plotted on each panel of Figure 3 by sinusoidal dotted yellow,

and light green curves, with periods of 40.0 and 34.8 minutes, respectively. The velocity amplitudes of the oscillations over the S1 and S2 slits are obtained to be 5.2 and 4.6 km/s, respectively.

The displacement amplitudes of the oscillations over the S1 and S2 slits obtained to be 12.5 and 9.6 Mm, respectively. To comparison, the Ballistic heights (h_B) due to the pure upward plasma injection with velocity of v is calculated as, $h_B = v^2/2g$. Considering the $g = 274\,m/s^2$, and velocity amplitudes of 5.2 and 4.6 km/s, the Ballistic heights obtained to be 0.05 and 0.04 Mm, respectively, which are about 250 to 240 times shorter than the observed displacement amplitudes of the observed oscillations. Therefore, another mechanism is required to eject and keep theses oscillations in the prominence structure.

The oscillations over the S1 and S2 slits seem to have a 180 degrees phase difference. However, at the ending part of the study (after the minute 80), while the filament eruption is progressing, it looks that the prominence dark area undergoes a similar (quite in phase) oscillating pattern. This happens because of the difference in the periods of the oscillations over the S1 and S2 slits ($\Delta T = 40.0 - 34.8 = 5.2\,min$), and their 180 degrees difference in their initial phase at the starting time of the study.

Another interesting fact is that the oscillatory patterns, over the each of the slits S1 and S2, exhibit an in-phase behavior for the all warm (171, 193 Å), and hot (211, 335, 94 Å) passbands, which might be an indication of iso-thermal structure for the prominence core. Further discussions are provided in the Section 4.

3.2 Upward propagating waves

Black, red, and blue lines in the Figs. 4 to 7 demonstrate the light curves of the selected twenty points in the Figure 2 for the AIA 171, 193, and 211 Å lines, respectively. Following the maxima and minima of a couple of oscillations in the light curves, it looks that they are functions of time and position, simultaneously. For instance,

- between the minutes 30 to 80 of the study (over the Figure 4), one can see three brightening pulses moving from the point 1 toward the point 5. Over-plotting the purple dot-dashed lines the group speed of the upward propagating wave (v_g, at which the energy of the wave getting transported) is estimated (from the gradient of the plotted line) to be equal to $13.4 \pm 0.9\,km/s$.

- Between the minutes 10 to 45 over the Figure 5, a similar pattern is observable for the two shorter intensity peaks, moving from the point 6 toward the point 10. This upward moving perturbation is tracked by the over-plotted the purple dot-dashed lines with slopes of about $v_g = 12.9 \pm 0.9\,km/s$.

- Between the minutes 60 to 90 over the Figure 6 a similar pattern is repeated from the point 11 toward the point 15, with a velocity of $11.3 \pm 0.8\,km/s$ (purple dot-dashed lines).

- In time intervals of 70 to 95 minutes, two intensity peaks travel from the point 16 toward the point 20, with propagating speeds of $19.5 \pm 1.6\,km/s$ (demonstrated by purple dot-dashed lines). The group speeds are summarized in the Table 1.

The upward propagating wave pattern is observable in the all the three studied wavelengths, with a slight time delay in their peak intensity emergence time. In some cases, the intensity peak first appears in the cooler channel (AIA 171 Å, $\log[T] \sim 5.8$), and then warm up to hotter passbands of (AIA 193 Å, $\log[T] \sim 6.1$), and (AIA 211 Å, $\log[T] \sim 6.3$), respectively. Three examples of such heating cases are denoted by orange arrows on the Figure 4. However,

Table 1: Group speeds of the detected upward and downward propagating waves.

position	upward propagating wave (km/s)	**downward propagating wave** (km/s)
points 1 to 5	13.4 ± 0.9	24.2 ± 1.7
points 6 to 10	12.9 ± 0.9	23.3 ± 1.7
points 11 to 15	11.3 ± 0.8	20.4 ± 1.6
points 16 to 20	19.5 ± 1.6	19.5 ± 1.6

a couple of reverse processes (cooling from AIA 211 Å to AIA 171 Åchannels) are observed, as well. Three samples from the last processes are shown by dark-blue arrows on the Figure 4. Interestingly, the average time scales for the heating and cooling processes are quite short and in the range of about one minute. In the few cases, all the intensity peaks occur at a same instance, denoting the plasma having a multi-thermal structure.

3.3 Downward propagating waves

Using the same method, a couple of downward propagating waves observed over the all three studied wavelengths (AIA 171, 193, and 211 Å). For instance,

- between the time intervals of 80 to 110 minutes, the red dotted lines demonstrate a couple of intensity peaks, in all the three channels, propagating downward from the point 5 toward the point 1, over the top border of the studied prominence core. The both heating (orange arrows) and cooling (dark blue arrows) processes are observed during the mentioned downward propagating phase (Figure 4). At point 5 the third signal has a cooling nature (dark blue arrows), while, as it propagates and reaches to the point 10 it shows heating character (along with the middle signal, denoted by orange arrows).
- A multi-thermal short intensity peak propagates downward, from the point 10 toward the point 6, in the time intervals of 95 to 105 minutes (red dotted lines, Figure 5).
- In the time intervals of 15 and 40 minutes, a downward propagating pulse with a heating nature moves from the point 15 toward the point 11 (indicated by the red dotted lines, Figure 6).
- A downward propagating signal with cooling nature starts from the point 20 and moves toward the point 15, after the minutes 100 in the study time interval.

3.4 Nature of the detected propagating waves

Since the intensity is changing over the observed propagating waves, they could not be signatures of the Alfvén waves. So far, we have obtained an estimation about the velocities of the observed propagating waves. However, to distinguish the mode(s) of these waves, one needs to have an estimation about the magnetic field strength and electron density inside and outside of the prominence the structure, as well. Ghiasi et al. 2023 studied the spectral properties of the same prominence structure using the EIS/HINODE spectrometer data. They measured the magnetic field strength along the axis of this core prominence, and the electron density over the prominence structure to be about 3 Gauss, and $N_e = 2.0 \times 10^9\, cm^{-3}$, respectively [24]. Using version 7.1.3 of CHIANTI atomic database, the outside electron

density obtain to be $N_e = 1.9 \times 10^8\, cm^{-3}$. The direction of the propagation of these upward and downward waves is parallel to the axis of the core prominence structure (perpendicular to the solar surface), which is the same as the magnetic field direction in the prominence structure. Therefore, the detected waves should have a longitudinal nature. Consequently, the possibility of being a fast magneto-acoustic wave is ruled out. The only remained choice is the existence of the propagating slow magneto-acoustic waves. In this case, the following relation should be seen,

$$\frac{\rho_{out}}{\rho_{in}} = \frac{v}{C_s}$$

where, the ρ_{in}, ρ_{out}, v, and C_s denote the internal and external densities, the observed propagating velocity, and the sound speed, respectively [6]. Regarding the obtained electron densities inside, and outside of the prominence core, the observed propagating velocities should be equal to $0.095\, C_s$. The sound speed over the formation temperature of AIA 171, 193, and 211 Å passbands are 117, 165, and 208 km/s, respectively. Therefore, the observed propagating velocities should be in the range of 11 to 20 km/s, which are in a good agreement with our findings (Table 1).

Antolin et al. 2018 studied the downflows and upflows over the loop-like structures stemming from the studied prominence core and found that the collision of these counter-streaming flows (with energies of about $10^7 - 10^8\,\mathrm{erg/cm^2/s}$) could produce transverse MHD waves, with velocity amplitudes of about 40.0 km/s [25]. They estimated the magnetic field strength of the loop-like structures to be between 3.4 to 6.5 Gauss, which is in agreement with values obtained by Ghiasi et al. 2023 [24].

Zhou et al. 2018 performed a 3D MHD simulation over a prominence flux rope. They found magneto-acoustic longitudinal waves with a period of 49 minutes, along with two horizontal and vertical transverse oscillations with periods of 10 and 14 minutes [26].

4 Discussion and summary

The oscillatory nature of a limb core prominence is studied using AIA/SDO images. The main obtained results could be summarized as:

- The dark structure of the core prominence in AIA 171, 191, 211, 335, and 94 Å passbands observed to have vertical oscillations with periods of 40.0 and 34.8 minutes over the slits S1 and S2, with velocity amplitudes of 5.2 and 4.6 km/s, respectively. Different mechanisems, such as, gravitational disturbances, pressure imbalance, or magnetic tension are beleived to be the possible driving agent(s) of such vertical oscillations [2,27–29]. The observed oscillations seems to be parallel to the magnetic field axis of the prominence core structure, indicating the type of the oscillation to be longitudinal. Ghiasi et al. 2023 estimated the magnetic field along the axis of this core prominence to be about 3 Gauss [24]. They observed a transverse kink and sausage oscillations over the same structure, simultaneously. Obtaining a 27 degrees inclination for the magnetic field direction, respect to the plane of sky, they obtained the kink amplitude velocity and period of 5.3 km/s, and 33.4 minutes, respectively. The kink period of 33.4 minutes is very close to those of found in this study (40.0 and 34.8 minutes) over the prominence core. A possible explanation could be the projection effect which may cause the peak of the kink wave to be observed as vertical oscillations (respect to the surface of the sun); Moving the kink peak could move the position of the brightness over the structure and creates oscillatory pattern, as it is observed. In this case, the

observed amplitude velocities have to be related as,

$$v_{\text{Amp. vel.}} = v_{\text{Amp. kink}} \cos(27^\circ) = 5.3 \cos(27^\circ) = 4.7\,\text{km/s}$$

which is very similar to those of found in this study.

- These long period oscillation started 54 minutes before an external flare eruption starts to develop over the north side of the studied core prominence, and continued for about two hours. Wave fronts from the flare eruption might be the exciter agent of these long period oscillation over the entire core prominence structure. Propagating wave fronts of the flare, would impact the middle part (or the entire) of the core prominence. If they would act as a heating source, the temperature of the prominence structure would rapidly rise and fall, due to the thermal balance between the injected heating and heating loss through conduction and viscosity, as it is shown by Priest and Forbes 2002 [3,30]. The multiple rapidly heating and cooling effects (denoted on Figure 4 by the orange and dark-blue arrows), with the time scales less than one minutes, would support this idea.
- Both the top and bottom borders of the prominence core, over the slits S1 and S2, show the evidence of upward and downward propagating waves (Figs. 4 to 7) with velocities in the range of 11.3 to 24.2 km/s. The nature of these oscillations are distinguished as slow magneto-acoustic waves.

Acknowledgment

Data are courtesy of NASA/SDO and the AIA science teams.

Authors' Contributions

All authors have the same contribution.

Data Availability

No data available.

Conflicts of Interest

The authors declare that there is no conflict of interest.

Ethical Considerations

The authors have diligently addressed ethical concerns, such as informed consent, plagiarism, data fabrication, misconduct, falsification, double publication, redundancy, submission, and other related matters.

Funding

This research did not receive any grant from funding agencies in the public, commercial, or nonprofit sectors.

References

[1] Foukal, P. V. 2004, Solar Astrophysics, WILEY-VCH: Royal Swedish Academy of Sciences.

[2] Arregui, I., Oliver R., & Ballester J. L. 2018, Living Review in Solar Physics, 15, 3.

[3] Priest, E. R. 2014, Magnetohydrodynamics of the Sun, Cambridge University Press.

[4] Kazachenko, M. D., Canfield, R. C., Longcope, D. W., & Qiu, J. 2012, Sol. Phys., 277, 165.

[5] Aschwanden, M. J. 2019, New millennium Solar Physics, Springer: Astrophysics and Space Science Library.

[6] Aschwanden, M. J. 2005, Physics of the Solar Corona, Springer: Praxis Publishing Ltd, Chichester, UK.

[7] Parenti, S. 2014, Living Reviews in Solar Physics, 11, 1.

[8] Isobe, H., & Tripathi, D. 2006, APJ, 449, L17.

[9] Pintér, B., Jain, R., Tripathi, D., & Isobe, H. 2008, APJ, 680, 1560.

[10] Bone, L. A., Van Driel-Gesztelyi, L., Culhane, J. L., Aulanier, G., & Liewer, P. 2009, Sol. Phys., 259, 31.

[11] Oliver, R. 1999, ESA Special Publication, ESA, Noordwijk.

[12] Engvold, Ø. 2001b, Proc 2001/Ballester, 123.

[13] Wills Davey, M. J., & Thompson, B. J. 1999, SP, 190, 467.

[14] Ofman, L., Nakariakov, V. M., & DeForest, C. E. 1999, APJ, 514, 441.

[15] Berghmans, D., & Clette, F. 1999, SP, 186, 207.

[16] De Moortel, I., Ireland, J., Walsh, R. W., & et al. 2002a, SP, 209, 61.

[17] De Moortel, I., Hood, A. W., Ireland, J., & et al. 2002b, SP, 209, 89.

[18] De Moortel, I., Ireland, J., Hood, A. W., & et al., 2002c, A&A, 387, L13.

[19] Gupta, G., Banerjee, D., Teriaca, L., Imada, S., & Solanki, S. 2010, ApJ, 718, 11.

[20] Yuan, D., & Nakariakov, V. M. 2012, A&A, 543, A9.

[21] Nakariakov, V. M., & Kolotkov, D. Y. 2020, ARA&A, 58, 441.

[22] Botha, G. J., Arber, T. D., Nakariakov, V. M., & Zhugzhda, Y. D. 2011, ApJ, 728, 84.

[23] Lemen, J. R., Title, A. M., Akin, D. J., & et al. 2012, Sol. Phys., 275, 1.

[24] Ghiasi, M., Dadashi, N., & Ebadi, H. 2023, MNRAS, (under revision).

[25] Antolin, P., Pagano, P., De Moortel, I., & Nakariakov V. M. 2018, APJL, 861, L15.

[26] Zhou, Y. H., Xia, C., Keppens, R., Fang, C., & Chen, P. F. 2018, APJ, 856, 179.

[27] Jing, J., Lee, J., Spirock, T. J., & Wang H. 2006, Sol. Phys., 236, 97.

[28] Luna, M., Diaz, A. J., & Karpen J. 2012a, APJ, 757, 98.

[29] Kuperus, M., & Tandberg-Hanssen, E. 1967, Sol. Phys., 2, 39.

[30] Priest, E. R., & Forbes, T. G. 2002, APJR, 10, 313.

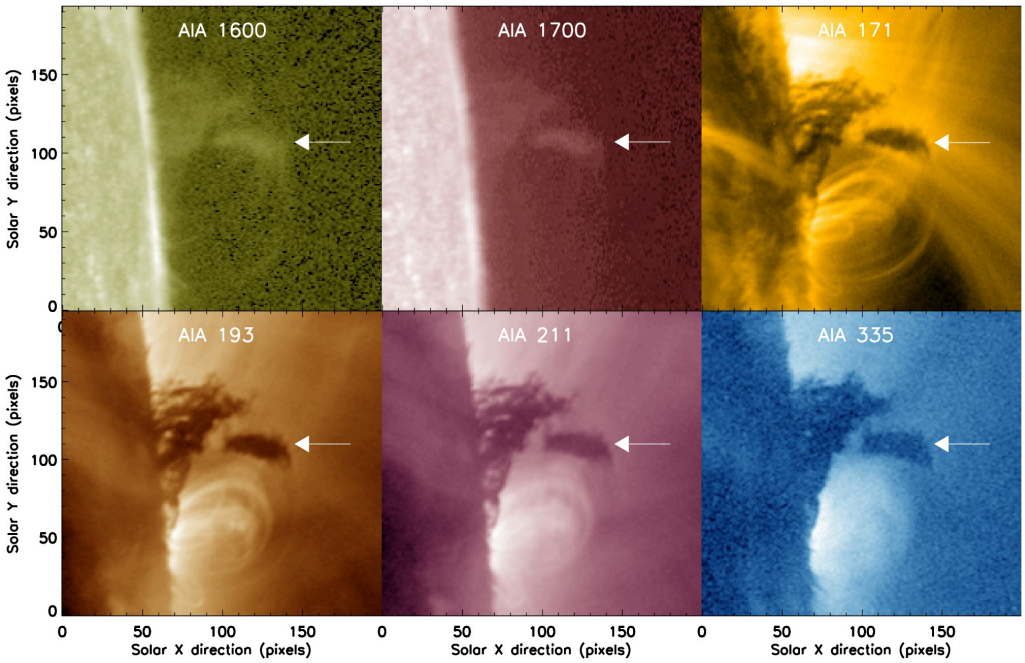

Figure 1: The studied prominence is represented in different AIA passbands, on the 3rd April 2014, 13:16:10 UT. White arrows show the position of the prominence core above the solar limb. The structure looks bright in the 1700, and 1600 Å channels. However, it looks darker over the other hotter channels (171, 193, 211, 335 Å).

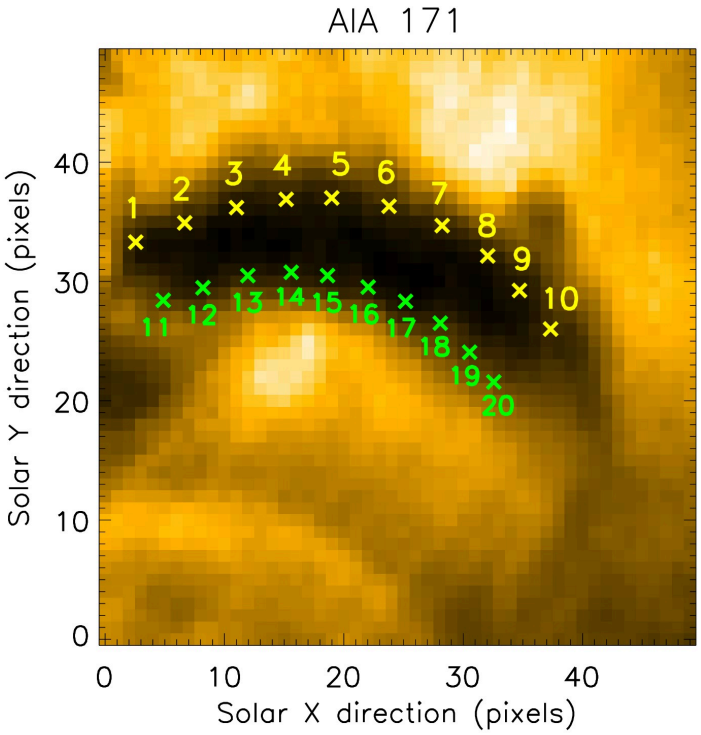

Figure 2: A closer look at the prominence core in AIA 171 Å channel, 13:32:10 UT. Twenty points are selected over the top and below borders of the structure. The light curves of the corresponding points are plotted in Figs. 4 to 7.

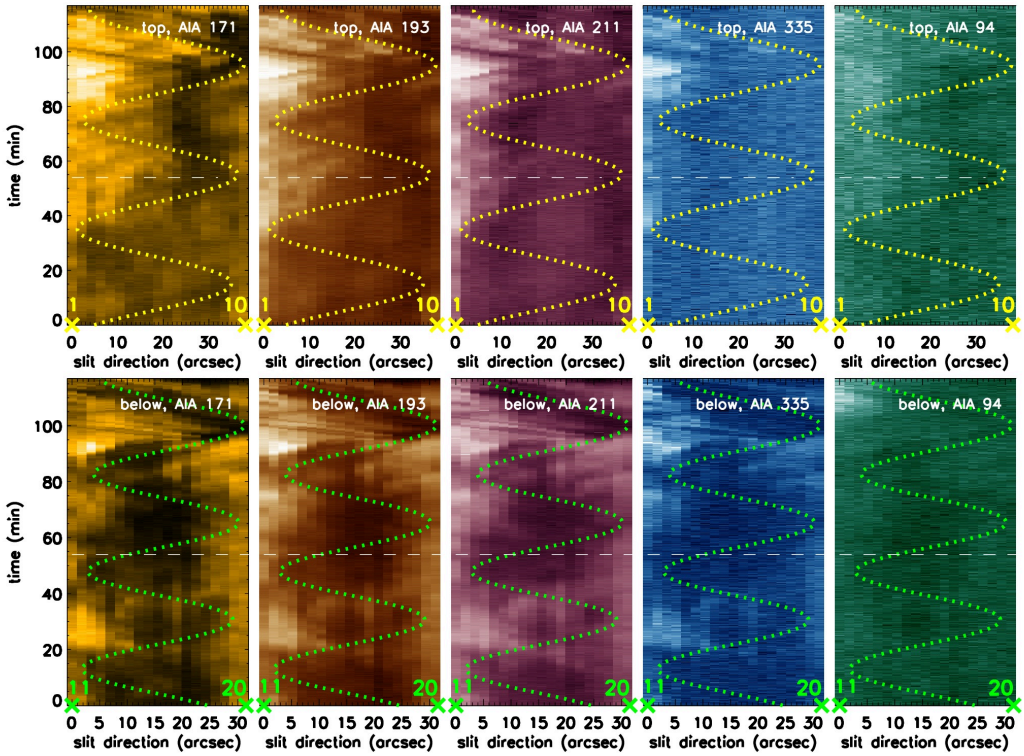

Figure 3: Top and bottom rows represent the time-distance plots of the artificial slit 1 (S1: from point 1 to point 10) and slit 2 (S2: from point 11 to point 20) in the AIA 171, 193, 211, 335, and 94 Å passbands, respectively. The white dashed lines demonstrate the starting instance of the Flare Eruption (FE) event occurred nearby the north side of the studied prominence core. The sinusoidal dotted yellow (T = 40.0min), and light green curves (T = 34.8min) are over-plotted (by-eye) to track the overall displacements of the dark prominence structure, respectively. The oscillations over the S1 and S2 slits seem to have a 180 degrees phase difference. The velocity amplitudes of the oscillations over the S1 and S2 slits are obtained to be 5.2 and 4.6 km/s, respectively.

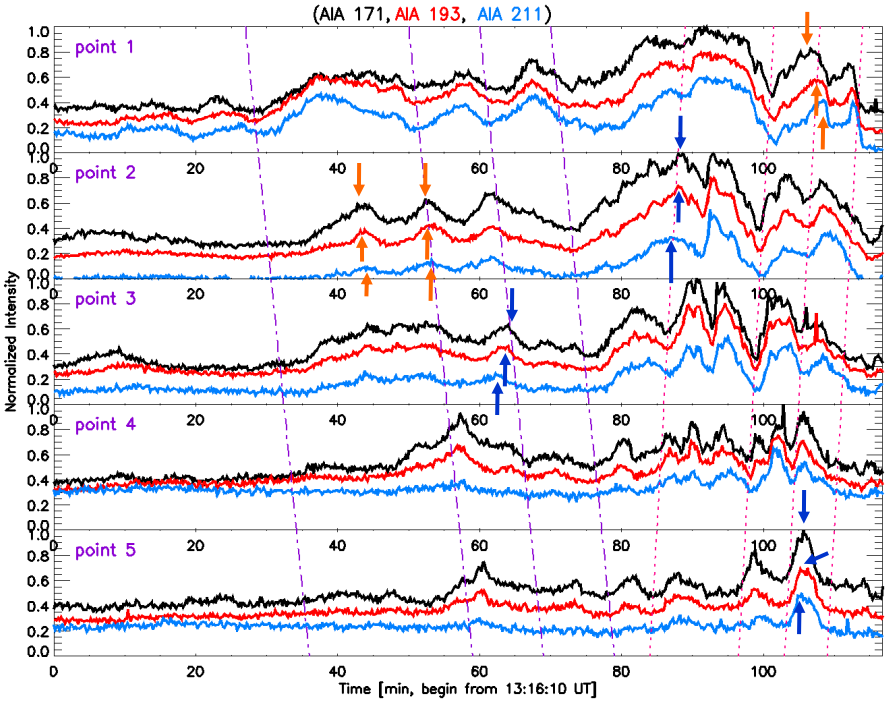

Figure 4: Top to bottom: Light curves of the points 1 to 5 (selected and marked in Figure 2) are plotted in the AIA 171, 193, 211 Å passbands. Pink dotted, and purple dot-dashed lines represent the downward and upward propagating waves along the prominence core structure, respectively.

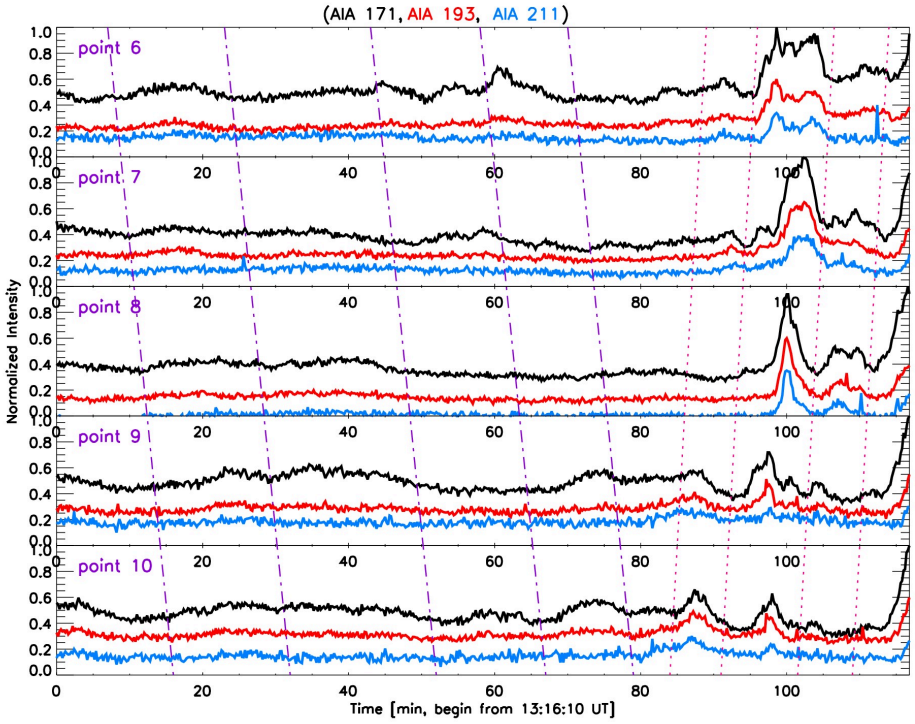

Figure 5: Analogous to Figure 4, but for points 6 to 10 points.

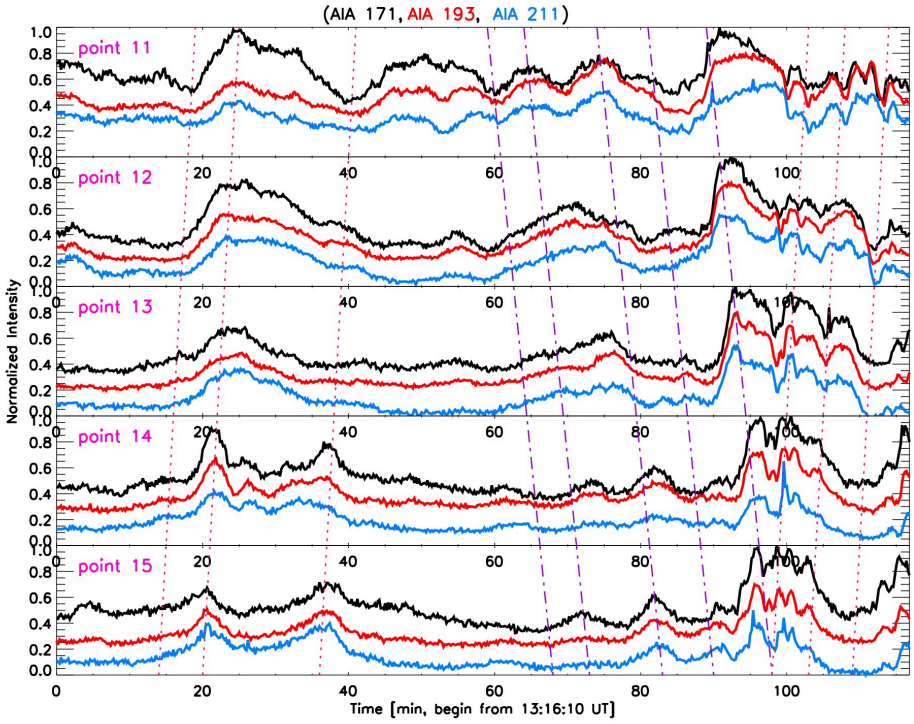

Figure 6: Analogous to Figure 4, but for points 11 to 15 points.

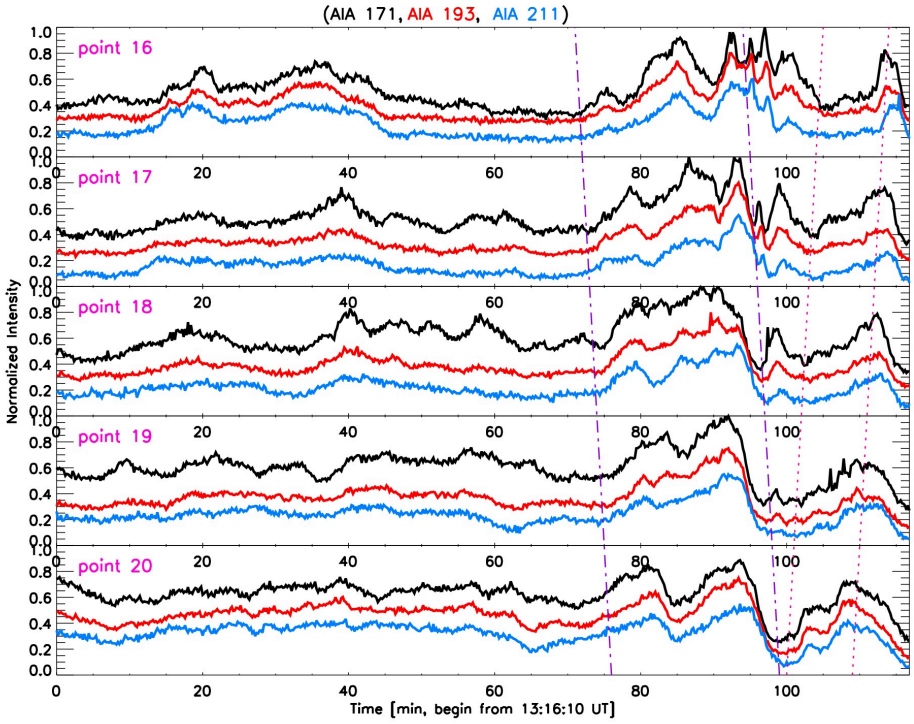

Figure 7: Analogous to Figure 4, but for points 16 to 20 points.